Applied Energy 254 (2019) 113574

Contents lists available at ScienceDirect

Applied Energy

journal homepage: www.elsevier.com/locate/apenergy

Lithium-ion battery overcharging thermal characteristics analysis and an impedance-based electro-thermal coupled model simulation

Junqiu Li*, Danni Sun, Xin Jin, Wentong Shi, Chao Sun*

Collaborative Innovation Center of Electric Vehicles in Beijing, Beijing Institute of Technology, Beijing 100081, China

HIGHLIGHTS

- An impedance-measurement-based method is proposed for heat generation calculation.
- An electro-thermal coupled overcharging battery model is built.
- A series of overcharging experiments are conducted for thermal abuse analysis.
- Accurate thermal simulation results can improve battery safety management.

ARTICLE INFO

Keywords:
Lithium-ion battery
Electro-thermal model
Overcharge
Experiment
Temperature

ABSTRACT

Overcharging is one of the main reasons causing lithium-ion battery thermal abuse, probably leading to vehicle accidents. This paper develops an impedance-based method to characterize the battery heat generation during overcharging process. An electro-thermal model is adopted for better computation efficiency. A series of overcharging experiments at 30 ℃ and 60 ℃ are conducted. Interestingly, three stages can be identified from the results, which are the normal heat-accumulating stage, fast heat-accumulating stage and thermal runaway stage, respectively (Stage I, II and III). During Stage I and II, pulse-relaxation and impedance-measurement methods are developed to parameterize the electro-thermal model, under different state of charge, temperature and charging rate conditions. Results of genetic algorithm with Hybrid Pulse Power Characteristic cycling data are used as benchmark. The simulated surface temperature results during overcharging are validated via experiments, which shows that medium frequency impedance method outputs better equivalent resistance and surface temperature estimation accuracy. The proposed model achieves to reduce the temperature estimation root mean squared error to under 0.9 ℃ in all overcharging situations, with greatly reduced computation complexity.

1. Introduction

With large-scale applications of lithium-ion batteries, the public have paid more attention to the safety issues especially in the field of electric vehicles and energy storage field [1]. Lithium-ion batteries use organic solution as electrolyte, which can easily decompose or even burn at high temperature conditions [2]. The solid-electrolyte interphase (SEI) film that protects the anode is a metastable structure [3]. It can easily decompose and release heat and gases at high temperature [4]. Anode material, which is unprotected, is more reactive and reacts with the solvent or binder in the electrolyte, releasing more heat [5]. The cathode material might release oxygen at high temperature, which would oxidize the electrolyte or cause combustion [6]. Under some extreme abused conditions, the occurrence probability of these side reactions is high, which increases the risk of thermal runaway [7].

At present, the main method to overcome the weakness of electric vehicle mileage is to increase the capacity of the power battery, but the increase in capacity will definitely affect the safety performance of the vehicle [8]. Large-capacity battery packs in an electric vehicle may experience more complex and harsher environments than electronic products during operation [9]. In order to protect the personal and property safety and solve safety technical obstacles for large-scale applications, the lithium-ion battery safety issues need to be further studied [10]. For example, repeated experiments are conducted to investigate the degree of thermal runaway damage for batteries [11]. Combined with a large number of experimental data, rigorous theoretical analysis is applied to find the cause and evolution of thermal runaway [12]. It is possible to set up early warning and prevention and

* Corresponding authors at: Collaborative Innovation Center of Electric Vehicles in Beijing, Beijing Institute of Technology, 5 Zhongguancun South Street, Haidian, Beijing, China.
E-mail address: lijunqiu@bit.edu.cn (J. Li).

https://doi.org/10.1016/j.apenergy.2019.113574
Received 23 August 2018; Received in revised form 21 May 2019; Accepted 17 July 2019
Available online 02 August 2019
0306-2619/

control methods at various stages of the thermal runaway process for batteries to prevent future damage [13].

1.1. Lithium-ion battery thermal safety

Lithium-ion batteries are sensitive to temperature [14]. High temperatures not only affect the discharge capacity but also cause great safety problems [15]. For example, the battery pack in an electric vehicle under the hot sun in summer, the power battery with internal heat dissipation failure at high rate discharge, or the battery in the base station in the hot zone, will experience a high temperature environment [16]. The battery is composed of a variety of materials, which have different decomposition reaction temperatures [17]. However, when multiple materials interact together, reactions occur at a lower onset temperature [18]. For example, when there is electrolyte, the exothermic peak appears at 150 °C in the reaction between the anode and the solvent. Whereas it does not appear until 300 °C in the absence of the electrolyte [19].

Qingsong Wang et al. studied the effect of initial temperature on thermal runaway, and found that when the battery is at high temperature (60 °C), its thermal stability is seriously weakened due to thermal degradation inside the battery, which indicates greater thermal runaway hazard [20]. Xuning Feng et al. found that before the thermal runaway occurred, the internal and external temperature difference did not exceed 1 °C, and the battery internal resistance slowly increased from 20 mΩ to 60 mΩ. However, after the thermal runaway occurred, the temperature difference increased to 520 °C with the maximum temperature of 870 °C. The internal resistance instantly increased to 370mΩ [21].

1.2. Lithium-ion battery overcharging safety

A battery pack in an electric vehicle is composed of a number of battery cells connected in series and parallel. Due to the inconsistency of the cells, the battery may be overcharged even during normal usage, let alone when the charging pile does not function correctly [22]. When the lithium-ion battery is fully charged, the lithium contained in the cathode has mainly been de-embedded and enters the anode, and the remaining lithium content is insufficient to support long-term overcharge [23]. When the lithium ion of cathode is completely de-embedded, the structure of the cathode material will be destroyed and the resistance will increase sharply, resulting with an increase in the ohmic heat production [24]. At the same time, an oxidation exothermic reaction near the cathode causes oxidation and decomposition of the electrolyte, thereby generating a large amount of heat and gas [25]. Since an excess of lithium cannot insert into the anode, it precipitates on the surface of the anode to form lithium dendrites [26]. Overlong lithium dendrites will pierce the diaphragm, causing a short circuit inside the battery, causing the battery to release a large amount of heat in a short time [27]. The rapid generation of these heat and gases can cause the battery to expand, bulge, and eventually cause the thermal runaway [28].

Hengwei Liu et al. found that the starting temperature of thermal runaway by overcharging was much lower than that by only increasing the ambient temperature. Thermal runaway occurred at 73.5 °C in the overcharge scenario, with the maximum temperature reached 450 °C [29]. Dongsheng Ren et al. proposed an overcharge-to-thermal-runaway model and found that the electrolyte oxidation reaction and reaction between deposited lithium and electrolyte were dominant in the heat generation during the overcharging [30]. QingFeng Yuan et al. found that the battery internal resistance increased 7.7 times during the overcharging. It was inferred that the lithium dendrite deposited on the anode was the main cause of thermal runaway [31]. Finegan found that the thickness of the positive lithium cobalt oxide material increased after overcharging [32]. Yadong Liu et al. found that overcharge destroyed the electrode surface of the battery and the impedance increased [33].

1.3. Contribution of this paper

Most existing studies concentrate on thermal runaway modeling of batteries via side reactions of the internal materials [1]. However, side reactions of lithium-ion batteries are extremely complicated and hard to capture its dynamics. We intend to develop an effective and equivalent method for thermal modeling, especially when the battery is overcharged. This paper proposes a novel method based on impedance spectroscopy measurement for heat generation characteristics analysis and simulation during the overcharging process before thermal runaway. An electro-thermal coupled model is adopted to reduce the dynamics complexity. A series of overcharging experiments at 30 °C and 60 °C are performed. The pulse-relaxation, medium frequency (MF) and low frequency (LF) electrochemical impedance methods are used to measure and identify the ohmic impedance changing within the battery. An electro-thermal model based on the Bernardi [34] model is established to simulate the temperature and voltage variation, using the above three resistance measurement methods. Furthermore, we employed genetic algorithm for accurate parameter identification of the equivalent circuit model and surface temperature as benchmark. The main contributions of this paper are listed as follows.

- A novel impedance-measurement-based method is proposed for lithium-ion battery heat generation calculation during the overcharging process, with an electro-thermal coupled model used.
- A series of experiments are conducted for thermal abuse analysis. Three stages of battery temperature variation are identified during overcharging.
- Equivalent resistance estimation by MF impedance is able to achieve the best model accuracy, with RMSE as low as 1.1 °C. By using genetic algorithm for parameterization, RMSE is further reduced to under 0.9 °C.

The remainder of the paper is organized as below. Section 2 introduces the experiment setup and main results. Section 3 proposes the lithium-ion battery electro-thermal coupled model, followed by the parameterization process depicted in Section 4. Section 5 presents the major simulation results and comparison with experimental data, with Section 6 drawing our main conclusions.

2. Surface temperature observation of overcharged battery

2.1. Experiment setup

A series of overcharging experiments have been conducted on a 35Ah lithium manganate battery $LiMn_2O_4$ to parameterize and establish the electro-thermal coupled model. A KIKUSUI PWR1600L DC power supply is used for the charging tests and a Fluke 2638A data acquisition instrument is used to collect the battery voltage, current, temperature, etc. The batteries are placed in an Ykytech thermal chamber, which is able to maintain the temperature between −55 °C to 150 °C. A Zahner Zennium electrochemical workstation is used for measuring impedance spectroscopy. The experiment setup, tested battery and experiment equipment are shown in Fig. 1(a)–(c), respectively. As it is very hard to measure the core temperature of lithium-ion battery without any destruction of the battery structure, we only measure its surface temperature.

The relevant specifications of the battery are shown in Table 1.

2.2. Battery temperature observation results

This paper's target is to investigate the thermal dynamics of lithium-ion battery during overcharging process. The overcharging experiment is conducted after three full constant C-rate discharging and Constant

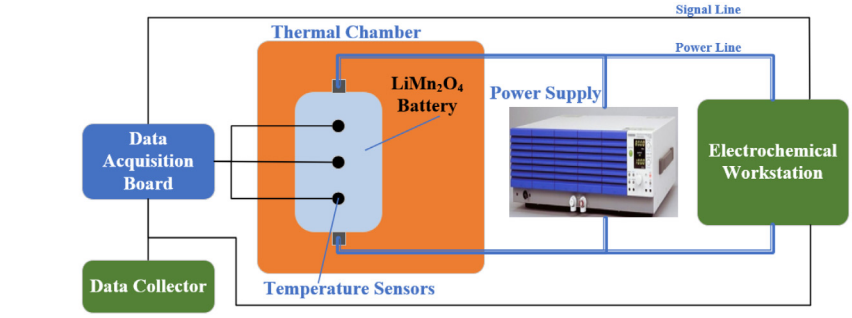

(a) Experiment setup

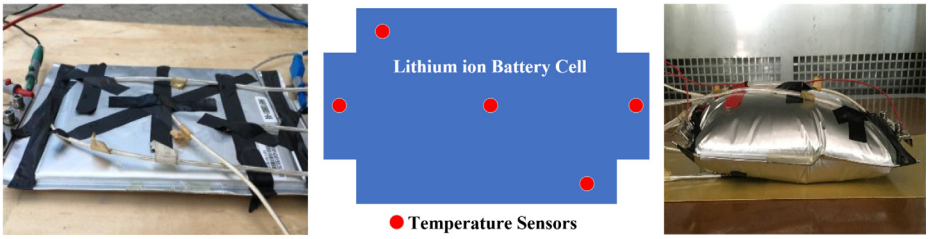

(b) Normal and Overcharged $LiMn_2O_4$ battery

(c) Experiment equipment

Fig. 1. Experiment setup, the tested battery and equipment.

Table 1
Specifications of 35Ah lithium manganate battery.

Specifications	Values
Rated Capacity	35Ah
Rated voltage	3.8 V
Cutoff voltage range	3.0–4.2 V
Energy Density	145 Wh/kg
Battery body size	195 × 167 × 13 mm
Mass	1.02 kg

Current Constant Voltage (CCCV) charging cycles till the battery SOC reaches 100%. Eight Pt100 temperature sensors are taped on each side of the battery surface to record the thermal dynamics. The overcharging experiment is performed under two ambient temperature conditions: 30 °C and 60 °C. At each ambient temperature, we overcharge the battery with 0.5C and 1C, respectively. The measured temperature curves under 0.5C overcharging at 30 °C are illustrated in Fig. 2, together with the temperature variation. Three stages were identified from the surface temperature data.

Stage I is normal heat accumulating stage. Battery voltage and temperature increasing rate was relatively slow. The surface temperature grew to 50 °C within the first 3700 s. The rising rate of surface temperature was generally lower than 0.025 °C/s. During this stage, the battery didn't swell, and there was no gas coming out. Researchers usually consider that there were no side reactions at this stage [35].

Stage II is fast heat accumulating stage. From the observed data in Fig. 2, we can see the battery surface temperature is obviously much higher than Stage I, and grew to nearly 70 °C within less than 500 s. The rising rate of surface temperature was between 0.04 °C/s and nearly 0.1 °C/s, which was much faster than Stage I. Moreover, some gas, such as CO_2 and H_2O, began to leak out of the battery package and the battery started to swell. It is known that the decomposition of electrolyte and solid electrolyte interface (SEI) layer is why there were gas leaking and swelling. According to the study of [31], a surface deposition layer on top of the anode electrode was detected at 160% SOC, which is assumed as plated lithium dendrite. Lithium ions gradually accumulated near the negative electrode, forming lithium dendrites, and the growth of dendrites began to damage the cell structure, leading to an increased internal resistance and eventually fast heat accumulation. Although the surface temperature is only 70 °C, the core temperature can be as high as 150 °C according to previous studies [36].

It should be noted that we included thermal runaway into Stage II. This is because thermal runaway always involves battery burning or explosion, which however is usually very short and fast. It is very difficult to distinguish thermal runaway process from heat accumulation process. The Stage I as a period before the thermal runaway can be used as an early warning signal.

Stage III is heat dissipation stage after severe thermal runaway. When the tested lithium-ion battery stopped explosion or burning, its package was greatly damaged. It is impossible to continue overcharging. The battery started to cool down slowly to the ambient temperature. From Fig. 2 we can see that the temperature variation is negative from time 4100 s, indicating reactions inside the battery stopped.

Fig. 3 demonstrates more surface temperature observation results of

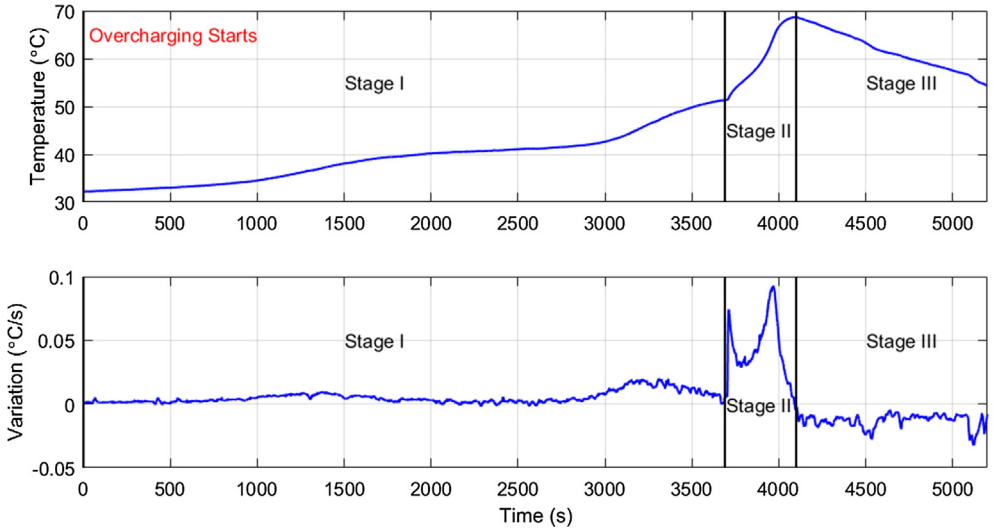

Fig. 2. Surface temperature and variation measured of 0.5C overcharging at 30 ℃.

the tested battery at different overcharging rates and ambient temperatures. We can see the 3-stage temperature changing pattern happened in nearly all the overcharging tests. In the 30 ℃ ambient temperature scenario, all overcharging surface temperatures increased up to over 62 ℃. The higher charging rate was used, the faster battery temperature grew. When the ambient temperature is changed to 60 ℃, similar results were observed. Interestingly, the peak temperature rose up to 75 ℃, but the rising rate is slower than 30 ℃ ambient temperature case. We infer this is because when the ambient temperature is higher, lithium ions are more active so that the internal resistance becomes smaller. Thus, the heat accumulation caused by the internal resistance is slower, leading to a reduction of temperature rising rate. So it becomes harder for the battery surface temperature to grow. All batteries swelled during the overcharging experiments.

3. Electro-thermal coupled model

In this paper, we developed an electro-thermal coupled approach to model the thermal dynamics of Stage I and Stage II for lithium-ion batteries. The ohmic resistance, polarization resistance and SEI resistance are captured by an equivalent circuit model. A three-dimensional thermal model is adopted to estimate the surface temperature of the battery cell, with side reactions considered. The equivalent circuit model and thermal model are introduced as the following.

3.1. Equivalent circuit model

Based on the electrochemical reaction mechanism of the battery, an equivalent circuit model in frequency domain is established as shown in Fig. 4. Assume R_{ohm} is the ohmic resistance, R_{ct} represents polarization resistance, R_{SEI} is the solid electrolyte interphase resistance (SEI), C_{dl} is the electric double-layer capacitance and C_{SEI} is the capacitance of SEI.

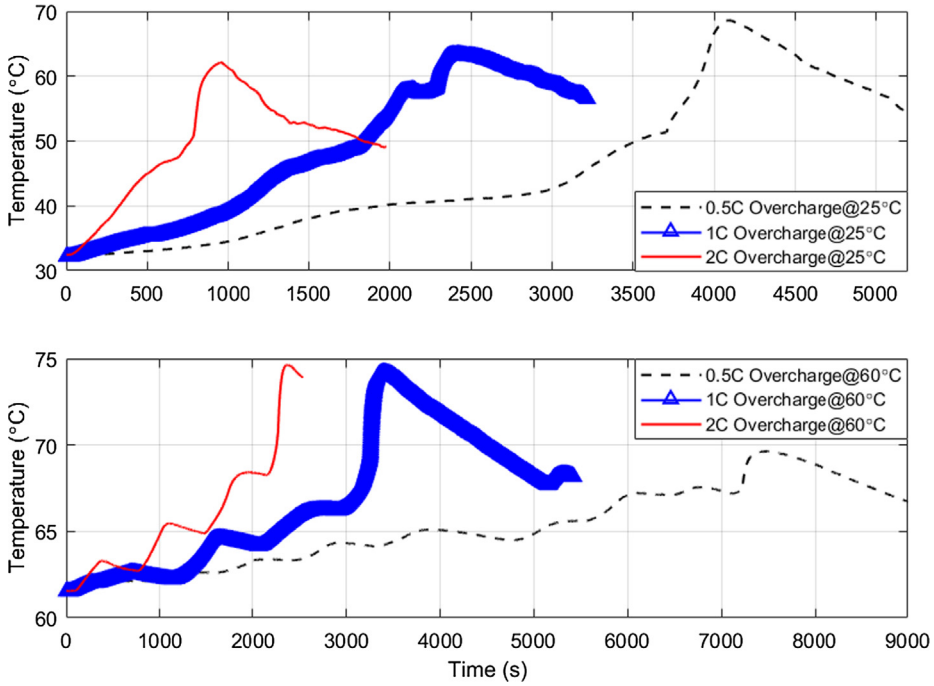

Fig. 3. Measured lithium-ion battery surface temperature at different overcharging rates.

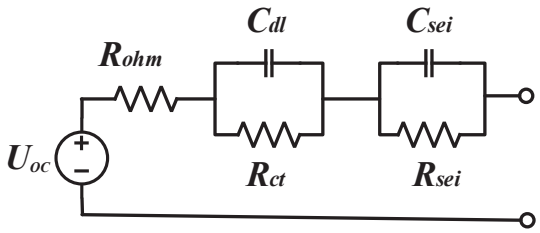

Fig. 4. Equivalent circuit model for lithium-ion battery.

Table 2
Details of side reaction parameters.

Parameters	Descriptions	Values
A_{sei}	SEI film decomposition reaction frequency factor	1.667E15 (s^{-1})
A_{ne}	Negative reaction frequency factor	2.5E13 (s^{-1})
A_{pe}	Positive reaction frequency factor	6.667E13 (s^{-1})
A_{e}	Electrolyte reaction frequency factor	5.14E25 (s^{-1})
$E_{a,sei}$	SEI film decomposition reaction activation energy	1.3208E5 (J/mol)
$E_{a,ne}$	Negative reaction activation energy	1.3308E5 (J/mol)
$E_{a,pe}$	Positive reaction activation energy	1.396E5 (J/mol)
$E_{a,e}$	Electrolyte decomposition reaction activation energy	2.74E5 (J/mol)
c_{sei0}	SEI film decomposition reaction initial value	0.15
c_{neg0}	Negative reaction initial value	0.75
α_0	Positive reaction degree initial value	0.04
c_{e0}	Electrolyte decomposition reaction initial value	1
z_{sei0}	SEI film thickness initial value	0.033
H_{sei}	SEI film decomposition reaction unit weight heat generation rate	257 (J/g)
H_{ne}	Negative reaction unit weight heat generation rate	1714 (J/g)
H_{pe}	Positive reaction unit weight heat generation rate	314 (J/g)
H_{e}	Electrolyte decomposition reaction unit weight heat generation rate	155 (J/g)
W_{c}	Negative electrode unit volume carbon content	6.104E5 (g/m^3)
W_{p}	Positive electrode unit volume active material amount	1.221E6 (g/m^3)
W_{e}	Unit volume electrolyte content	4.069E5 (g/m^3)
m_{sei}	Reaction order of SEI film	1
$m_{ne,n}$	Reaction order of negative material	1
$m_{pe,p1}$	Reaction order of positive material	1
$m_{pe,p2}$	Reaction order of positive material	1

The Warburg diffusion impedance is neglected because it is very small in the frequency range (greater than 0.1 Hz) used in this study. The role of the inductance is obvious especially in the high-frequency region, and has little effect on the real part of the impedance. Therefore, the inductance is ignored. During the overcharge process, the heat generation rate is related to the real part of the impedance.

The real part of the impedance can be expressed as

$$Z_{Re}(T,f) = R_{ohm}(T) + \frac{R_{ct}(T)}{1+(2\pi f)^2 R_{ct}^2(T) C_{dl}^2} + \frac{R_{sei}(T)}{1+(2\pi f)^2 R_{sei}^2(T) C_{sei}^2} \quad (1)$$

Table 4
The average thermophysical parameters.

Parameters	Descriptions	Values
ρ	Density	2055.2 kg/m^3
c	Specific heat capacity	1399.1 J/(kg·K)
k_x	Thermal conductivities in the x direction	29.557 W/(m·K)
k_y	Thermal conductivities in the y direction	29.557 W/(m·K)
k_z	Thermal conductivities in the z direction	0.89724 W/(m·K)
h	Convective heat transfer coefficient	54.7 $W/(m^2 \cdot K)$
ε [37]	Thermal radiant emissivity	0.07326

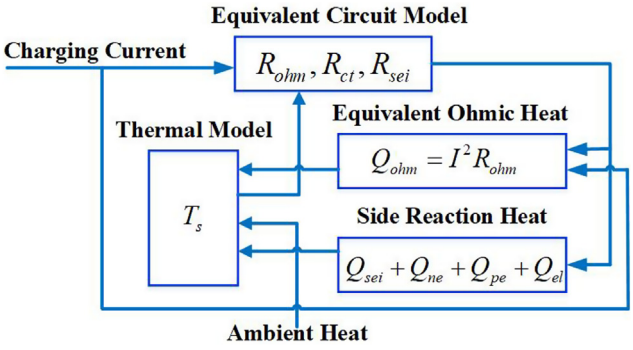

Fig. 5. Coupling mechanism of the electro-thermal coupled model.

3.2. Lithium-ion battery thermal model

The total heat generation Q_q is formulated as,

$$Q_q = Q_{rev} + Q_p + Q_{ohm} + Q_s \quad (2)$$

where Q_{rev} is reversible chemical reaction heat; Q_p is polarized heat; Q_{ohm} is ohmic heat, Q_s is the side reaction heat. According to the Bernaridi battery heat generation rate formula, the heat of reversible chemical reaction is determined by

$$Q_{rev} = -IT\frac{dE}{dT} \quad (3)$$

where I is current; E is open circuit voltage; T is Kelvin temperature. The polarization heat can be calculated by Eq. (4), where ΔU_p is the polarization voltage, which can be identified during overcharge.

$$Q_p = I \cdot \Delta U_p \quad (4)$$

Let R_{ohm} be the equivalent battery ohmic resistance, the ohmic heat can be calculated by,

$$Q_{ohm} = I^2 R_{ohm} \quad (5)$$

Side reaction heat is composed by four parts: SEI film decomposition heat Q_{sei}, anode reaction heat with solvent Q_{ne}, cathode reaction heat with solvent Q_{pe} and heat from electrolyte decomposition Q_{el}.

$$Q_s = Q_{sei} + Q_{ne} + Q_{pe} + Q_{el} \quad (6)$$

The SEI film is in a metastable state, and it is easy to decompose at higher temperature. Where R_{sei} is the decomposition rate; c_{sei} is a metastable lithium content; the thermodynamic constant

Table 3
Thermophysical parameters of each layer material in batteries.

Parameters	materials	thickness (um)	Density (kg/m^3)	Specific heat capacity(J/kg·K)	Thermal Conductivity W/(m·K)
cathode	$LiMn_2O_4$	55	2840	839	3.9
anode	graphite	55	1671	1064	3.3
separator	PVDF	30	659	1978	0.33
Positive current collector	Cu	10	8933	385	398
Negative current collector	Al	10	2710	903	208

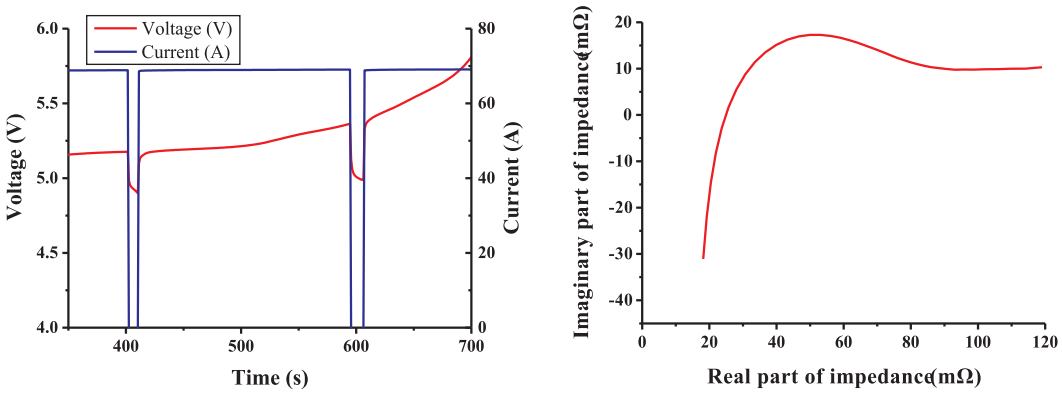

(a) Pulse-relaxation method (b) Electrochemical impedance method

Fig. 6. Pulse-relaxation method and electrochemical impedance method.

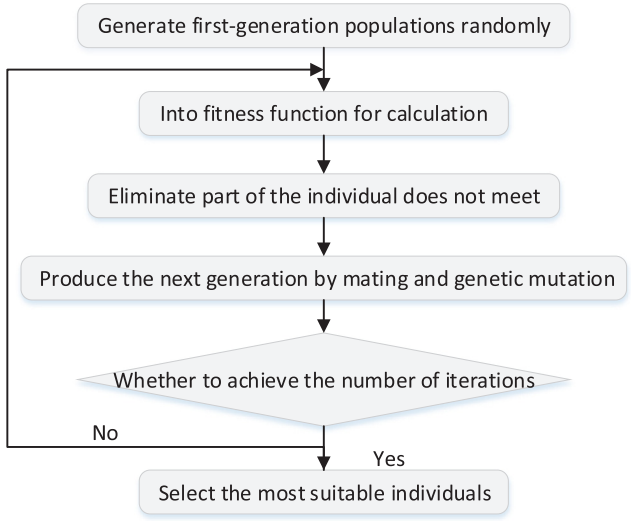

Fig. 7. Flow chart of genetic algorithm for parameter identification.

$R = 8.3145$ J gmol^{-1} gK^{-1}, then

$$Q_{sei} = H_{sei} W_c R_{sei} \tag{7}$$

$$R_{sei}(T, c_{sei}) = A_{sei} \exp\left[-\frac{E_{a,sei}}{RT}\right] c_{sei}^{m_{sei}} \tag{8}$$

$$\frac{dc_{sei}}{dt} = -R_{sei} \tag{9}$$

When battery temperature is very high, the lithium embedded in the negative electrode reacts with the solvent. Suppose R_{ne} is the reaction rate; z_{sei} is the thickness of the SEI film; c_{ne} is a dimensionless metastable lithium content.

$$Q_{ne} = H_{ne} W_c R_{ne} \tag{10}$$

$$R_{ne}(T, c_{ne}, z_{sei}) = A_{ne} exp\left(-\frac{z_{sei}}{z_{sei,0}}\right) \exp\left[-\frac{E_{a,ne}}{RT}\right] c_{ne}^{m_{ne}} \tag{11}$$

$$\frac{dc_{ne}}{dt} = -R_{ne} \tag{12}$$

Similarly, suppose α is reaction conversion rate; c_e is a dimensionless lithium concentration in the electrolyte.

$$Q_{pe} = H_{pe} W_p R_{pe} \tag{13}$$

$$R_{pe}(T, \alpha, c_e) = A_{pe} \alpha^{m_{pe,p1}} (1-\alpha)^{m_{pe,p2}} \exp\left[-\frac{E_{a,pe}}{RT}\right] \tag{14}$$

$$\frac{d\alpha}{dt} = R_{pe} \tag{15}$$

Assume R_e is the reaction rate. Decomposition reaction of electrolyte is given by

$$Q_{el} = H_e W_e R_e \tag{16}$$

$$R_e(T, c_e) = A_e \exp\left[-\frac{E_{a,e}}{RT}\right] c_e^{m_e} \tag{17}$$

$$\frac{dc_e}{dt} = -R_e \tag{18}$$

Other side reaction parameters are shown in Table 2 [1,30].

3.3. Three-dimensional heat transfer model

The heat generation of the battery before thermal runaway in the overcharge experiment is mainly ohmic heat and polarized heat. Only when the heat is accumulated to a certain degree in the later period to increase the temperature of the battery, the side reactions heat of SEI film, electrolyte, and the positive and negative is generated. Under the condition of overcharge abuse, a large amount of heat is generated inside the battery. The overcharge test of the entire battery can be regarded as an unsteady heat conduction process with an internal heat source. According to the basic law in three-dimensional heat conduction of heat transfer, the control equation of the three-dimensional thermal model is:

$$\rho c \frac{\partial T}{\partial t} = \frac{\partial}{\partial x}\left(k_x \frac{\partial T}{\partial x}\right) + \frac{\partial}{\partial y}\left(k_y \frac{\partial T}{\partial y}\right) + \frac{\partial}{\partial z}\left(k_z \frac{\partial T}{\partial z}\right) + Q_t \tag{19}$$

where ρ is the battery density; c is the specific heat capacity of the battery; k_x, k_y and k_z are the thermal conductivities in the ×, y, and z directions, respectively; T is the battery temperature; t represents the time; Q_t is the internal heat generation rate of the battery.

The initial conditions of the model are

$$T(x, y, z; 0) = T_0 \tag{20}$$

The heat exchange between the battery and the external environment is mainly convection heat transfer and heat radiation. Therefore, the boundary conditions of the battery thermal model control equation are:

$$-k\frac{\partial T}{\partial n}|_\Gamma = h(T - T_{amb}) \tag{21}$$

$$-k\frac{\partial T}{\partial n}|_\Gamma = \varepsilon\sigma(T^4 - T_{amb}^4) \tag{22}$$

where k is battery thermal conductivity; h is convective heat transfer coefficient; ε is thermal radiant emissivity; σ is the Stefan-Boltzmann

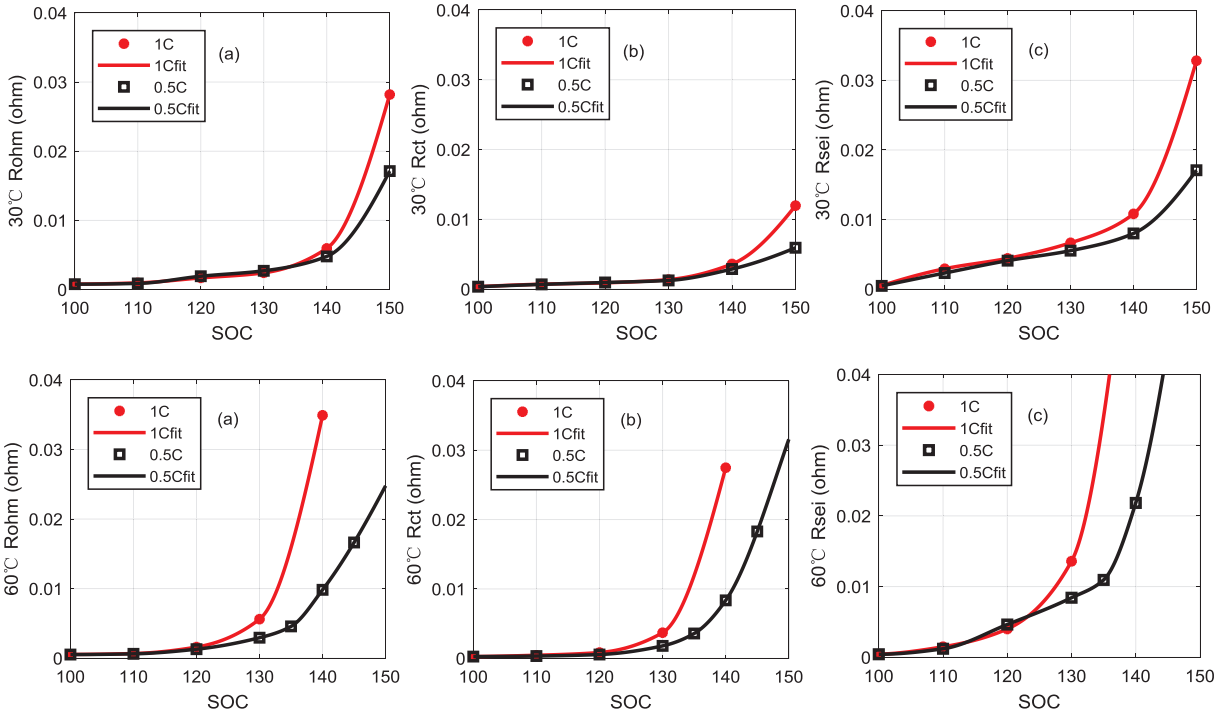

Fig. 8. Rohm, Rct and Rsei identified by genetic algorithm at 30 ℃ and 60 ℃.

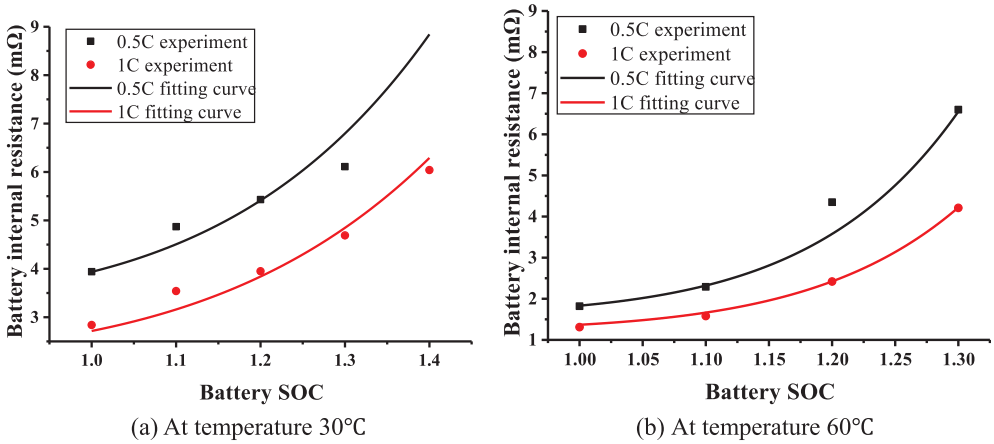

Fig. 9. Internal resistance measured with pulse-relaxation method.

constant of the battery heat radiation, $\sigma = 5.67 \times 10^{-8}\mathrm{W/(m^2 \cdot K^4)}$; T_{amb} is the ambient temperature.

Since the stacked lithium-ion battery materials are uniformly distributed in the width x and length y directions and layered in the thickness z direction, the battery is treated as an anisotropic material with the same thermal conductivity in the x and y directions and different thermal conductivity in the z direction in the three-dimensional thermal model.

The thermal conductivity is calculated by the parallel thermal resistance method in the length y and width x directions:

$$k_x = k_y = \frac{\sum L_i k_i}{\sum L_i} \tag{23}$$

The thermal conductivity is calculated by the series thermal resistance method in the thickness z direction:

$$k_z = \frac{\sum L_i}{\sum L_i / k_i} \tag{24}$$

where L_i is the thickness of each layer in the electrochemical model, k_i is the thermal conductivity of each layer material.

Thermophysical parameters of each layer material in batteries are shown in Table 3. The average thermophysical parameters of the battery are shown in Table 4.

The convective heat transfer coefficient h is identified by genetic algorithm. Because the blower of the thermal chamber is always on during the experiment, it is forced convection heat transfer condition. The forced convective heat transfer coefficient of air is about 20–100 $\mathrm{W/(m^2 \cdot K)}$. Therefore, it can be known that the value of the identified convective heat transfer coefficient$h = 54.7\ \mathrm{W/(m^2 \cdot K)}$ is reasonable.

3.4. Electro-thermal model coupling

It should be noted that during Stage I in Fig. 2, which is the normal heat accumulating stage, thermal runaway doesn't happen. From literature, we can know that heat from side reactions is not primary at this stage [30]. The battery heat mainly comes from irreversible ohmic heat. The Bernardi battery heat generation rate model based on the theory of

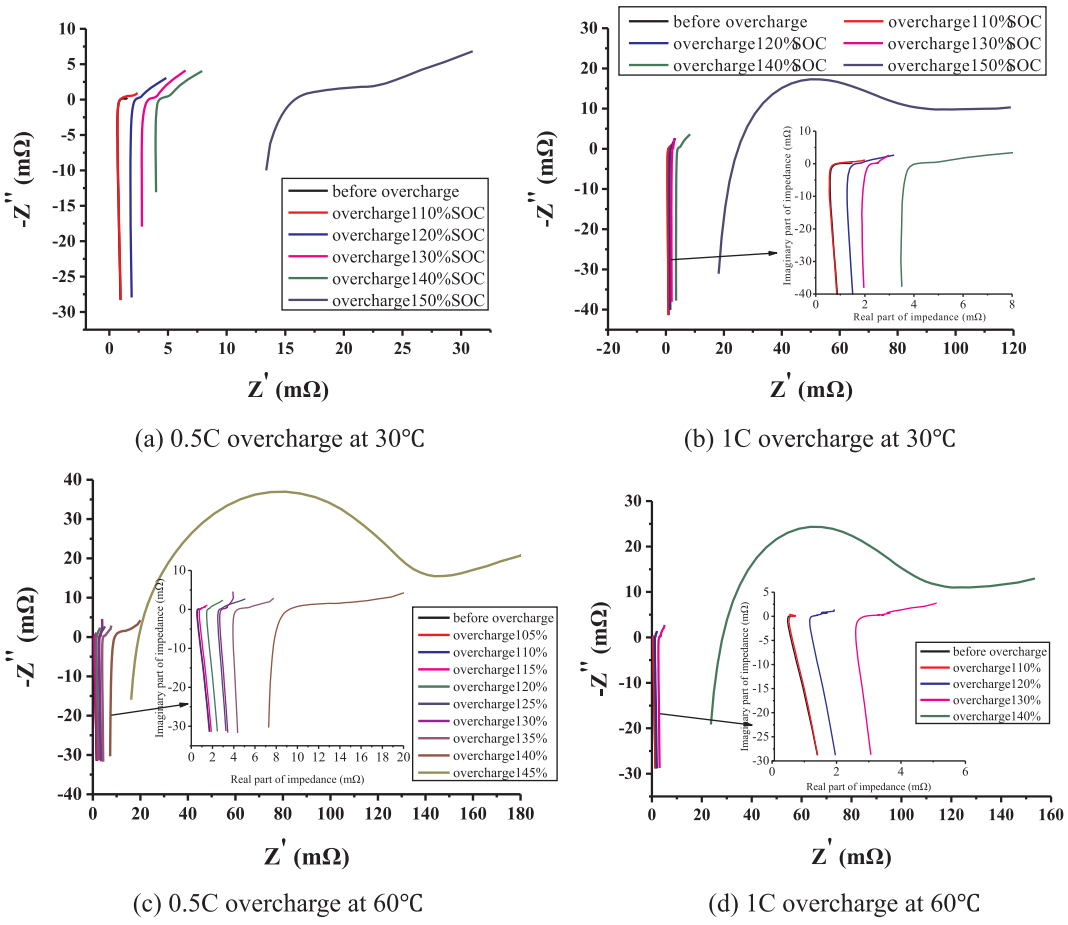

Fig. 10. Electrochemical impedance spectroscopy measured by electrochemical impedance method.

energy conservation is widely used to calculate the heat generation rate of the battery in Stage I. Thereafter, the paper computes the heat generation under overcharged condition by measuring the equivalent internal resistance by a pulse-relaxation method, a low-frequency AC impedance spectroscopy method and medium-frequency AC impedance spectroscopy method. Details of the methods can be found in Section 4.

However, as the overcharging process continues to Stage II of Fig. 2, which is the fast heat accumulating stage, we infer side reactions start to affect the thermal dynamics of the lithium-ion battery severely [38]. During this stage, we not only need to measure the equivalent internal resistance, but also need to calculate side reaction heat to improve the model accuracy. In one word, the thermal performance in Stage II is a coupled result of equivalent ohmic heat and side reaction heat.

In our paper, the equivalent circuit and thermal models interact through heat generation equations. We demonstrate this coupling mechanism in Fig. 5. The equivalent circuit model calculates the ohmic resistance, polarization resistance and SEI resistance of the battery for ohmic heat and side reaction heat calculation. In turn, the increase in temperature affects the parameters of the equivalent circuit model. Eventually, by using the equivalent ohmic heat and side reaction heat, we can accurately calculate the surface temperature of the battery T_s.

4. Parameterization of models

4.1. Equivalent internal resistance measurement

During the overcharging process, the electrochemical impedance and the internal resistance of the battery are measured for each overcharge period to calculate the heat generation rate of the ohmic heat, by two methods.

The first method is similar to [39], which identifies the internal resistance of the battery by briefly interrupting the overcharge process and obtaining the voltage drop after stopping the overcharge. We call it pulse-relaxation method, as shown in Fig. 6(a). The battery voltage decreases with time when the overcharge is interrupted, and the internal resistance of the battery can be identified according to the magnitude of the charging current and the voltage drop.

The ohmic internal resistance of a battery using this method can be calculated by Eq. (25), where ΔU_{ohm} is ohmic voltage drop, I is the overcharging current. Then we fit the measured results by Eq. (26), where a, b, c is the coefficient.

$$R_{ohm,1} = \Delta U_{ohm}/I \tag{25}$$

$$R_{ohm,2} = a \times (SOC)^b + c \tag{26}$$

The second method is to use an electrochemical workstation to measure the impedance spectroscopy of each stage of the battery overcharge, which is called electrochemical impedance spectroscopy method. The real part of medium-frequency impedance and low-frequency impedance are used to identify the ohmic resistance for the battery, which changes with the overcharge SOC. Then we fit the measured results also by Eq. (26).

By using the electrochemical workstation, the impedance of the battery is measured at regular intervals during overcharge. The measured impedance spectroscopy is shown in Fig. 6(b).

4.2. Parameter identification using genetic algorithm

The parameters of R_{ohm}, R_{ct}, R_{sei}, C_{dl}, C_{sei} in the equivalent circuit model need to be identified from experimental data. Here we employ

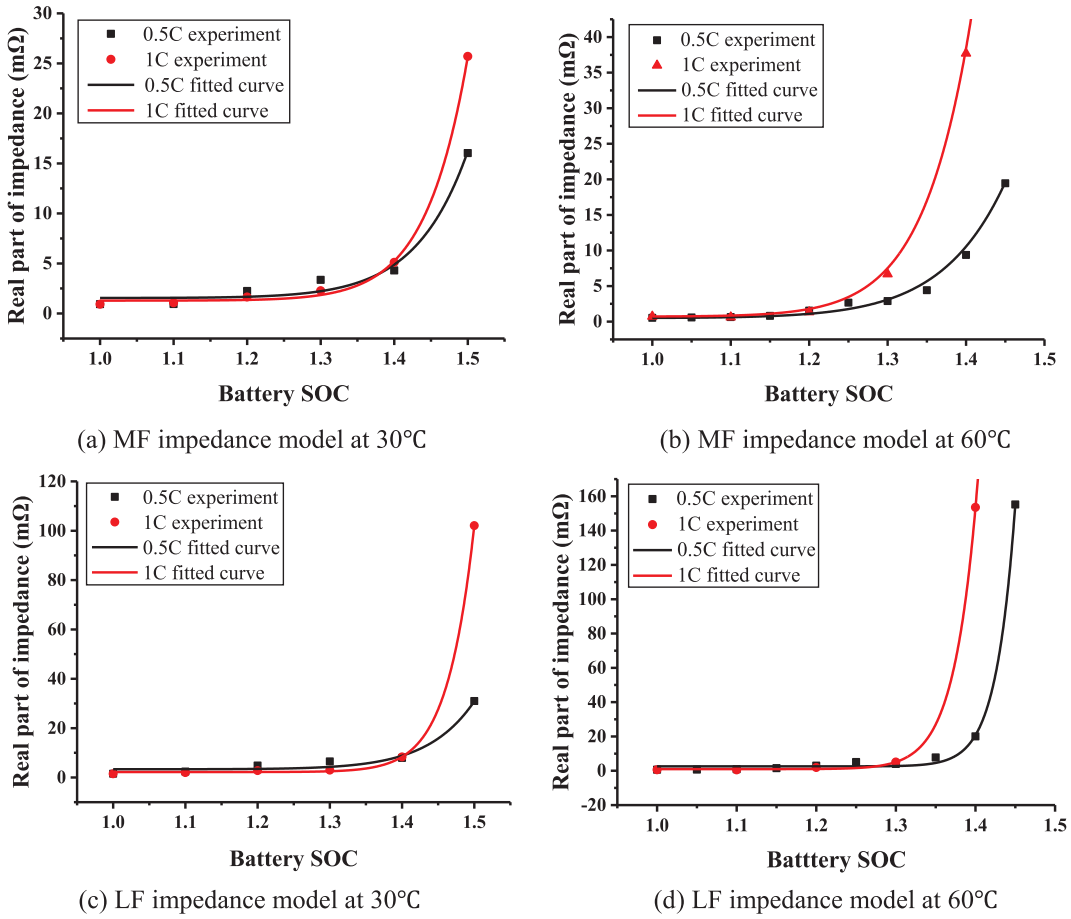

Fig. 11. The real part of impedance of the battery measured by the MF and LF impedance method.

genetic algorithm to determine these parameters and feed them back to the thermal model. The flowchart of genetic algorithm used in this paper is shown in Fig. 7. For the equivalent circuit model, the genetic algorithm fitness function is determined based on the least square principle of the calculated impedance and measured impedance.

$$J = \min\left\{\sum_{i=1}^{n} [Z(i) - Z_m(i)]^2\right\} \tag{27}$$

Fig. 8 shows the identified internal resistance by genetic algorithm, including the ohmic resistance, polarization resistance and solid electrolyte interphase (SEI) resistance. We can see that each part of the resistance increases approximately exponentially with the increase of SOC during overcharging.

5. Results and discussions

5.1. Equivalent internal resistance measurement results

The measured internal resistance with pulse-relaxation method is shown in Fig. 9. As can be seen, the ohmic resistance of the battery obtained by this method increases as the overcharge SOC increases, and decreases as the charge rate increases. The points in the Fig. 9 are measured values, and the curves are fitted results.

An electrochemical station was used to measure the impedance of the battery under different overcharge conditions, as stated in Section 4. The results are demonstrated in Fig. 10. From Fig. 10(a), we can see that after been overcharged to 110% SOC, the impedance spectroscopy of the battery mainly coincides with the impedance spectroscopy before overcharging. This indicates that the cathode of the battery still had lithium ions surplus after been fully charged. When the charging continued, the lithium ions of the cathode were still embedded in the graphite of the anode and the structure of the battery was not damaged.

However, as overcharge continued, the remaining lithium ions in the cathode become less and less. It was more and more difficult for the anode to embed lithium ions, so that a part of lithium ions deposited on the surface of the anode, which led to gradual increase of the battery internal resistance. The impedance spectroscopy gradually shifted to the right after been overcharged to 120% SOC. The real part of the impedance increased significantly, which caused an increase of the battery temperature. From Fig. 10(a), we can see when the battery was overcharged by 150% SOC, the real part of impedance of the battery increased by more than ten times, meaning the internal structure of the battery has been severely damaged by overcharging.

Similar results can be observed when the overcharging rate is set as 1C, as shown in Fig. 10(b). The impedance spectroscopy varied only slightly before 110% SOC. As the overcharging continued, the impedance spectroscopy shifted to the right, the real part of impedance gradually increased. Due to high temperature and voltage, side reactions happened within the SEI film, electrolyte, anode and cathode of the battery. Eventually a large amount of gas and heat accumulated inside the battery, causing thermal runaway. We can see the same pattern in Fig. 10(c)–(d), which demonstrates the measured impedance of 0.5C and 1C overcharging at 60 °C.

The internal ohmic resistance of the battery can be identified from MF electrochemical impedance spectroscopy [35]. When the imaginary part of impedance spectroscopy is zero, the corresponding real part of impedance is considered to be equal to the ohmic resistance of the batteryR_{ohm}. Fig. 11(a)–(b) shows the identified internal resistance while the battery was overcharging, as well as fitted curves.

Another method for calculating battery resistance by using

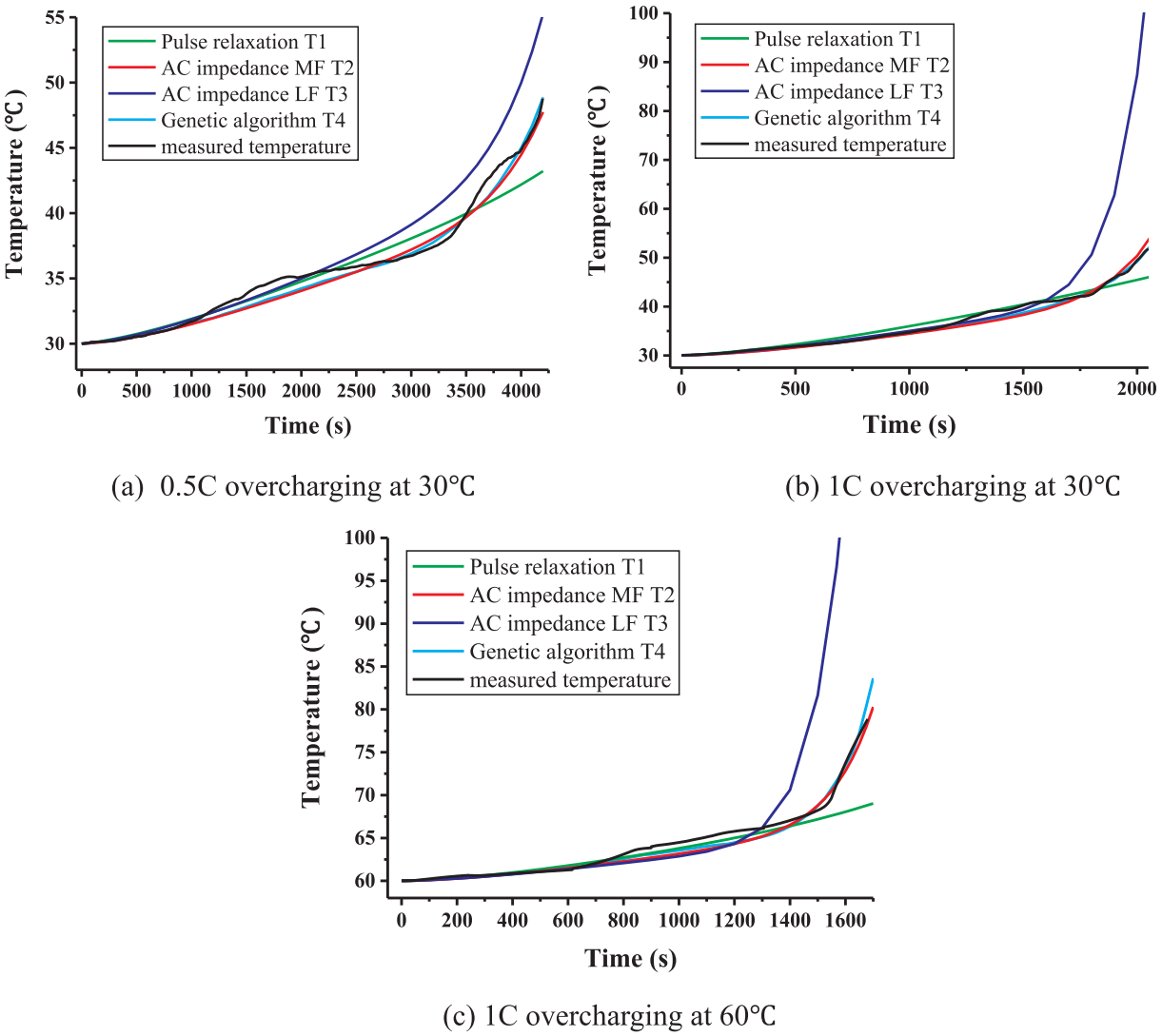

Fig. 12. Overcharged temperature rise curve simulated by different impedance identification methods.

Table 5
Accuracy evaluation of surface temperature by RMSE.

Approach	0.5C @ 30 °C	1C @ 30 °C	1C @ 60 °C
T1 - Pulse-relaxation	1.2548	1.5210	2.2990
T2 - AC impedance MF	0.7566	1.0281	0.8131
T3 - AC impedance LF	2.0917	14.9329	16.4300
T4 - Genetic algorithm identified	0.6468	0.6977	0.8120

impedance spectroscopy is to use the real part of impedance at a very low frequency. The real part of impedance at low frequency changes with SOC can be obtained at each impedance spectroscopy during the overcharge process. The results are shown in Fig. 11(c)–(d), as well as fitted curves.

5.2. Model validation

With the above electro-thermal coupled model, given parameters and identified internal resistance, it is able to calculate the surface temperature of tested lithium-ion battery cell. As elaborated in Fig. 5, during Stage I we mainly use equivalent ohmic heat to calculate the surface temperature. Whereas during Stage II, side reaction heat is included to increase the model accuracy. Here we assume,

- Surface temperature simulation result 1, noted as **T1**, is obtained by using the pulse-relaxation method for equivalent resistance calculation;
- Surface temperature simulation result 2, noted as **T2**, is obtained by using the medium frequency AC impedance spectroscopy for equivalent resistance calculation;
- Surface temperature simulation result 3, noted as **T3**, is obtained by using the low frequency AC impedance spectroscopy for equivalent resistance calculation;
- Surface temperature simulation result 4, noted as **T4**, is obtained by using the genetic algorithm for equivalent resistance calculation.

The overcharged temperature rise curve simulated by different impedance identification methods is demonstrated in Fig. 12. From Fig. 12(a) 0.5C overcharging at 30 °C, it can be found T1 temperature result rises nearly linearly, while T2 and T3 temperature results rise exponentially, especially during Stage II. When compared to experiment result, T2 reached the best performance. T4 result, using identified parameters from experiment data, also demonstrated better accuracy performance than T1 or T3. To further validate the effectiveness of our proposed model, we illustrated more results as below.

The 1C overcharging at 30 and 60 °C results in Fig. 12 showed that surface temperature by low frequency AC impedance spectroscopy method, that is T3, increased sharply. Especially during Stage II, which

is 1600–2000 s in the 30 ℃ case and 1300–1500 s in the 60 ℃ case, T3 deviated from the measured experiment temperature greatly. This result indicates that the identified equivalent internal resistance by low frequency AC impedance spectroscopy performs well during normal heat accumulating stage, however, not during the fast heat accumulating stage. The pulse-relaxation method is also not able to capture the thermal dynamics of lithium-ion batteries during overcharging.

Interestingly, T2 and T4 results both managed to follow the real surface temperature trajectory successfully. Intuitively, this result indicates that MF AC impedance spectroscopy is a better way to estimate the equivalent internal resistance of lithium-ion batteries. Moreover, the proposed equivalent circuit model and thermal model can mimic lithium-ion battery thermal dynamics with properly designed parameter identification method used.

The root mean squared error (RMSE) results compared with real surface temperature results are shown in Table 5. Pulse-relaxation method managed the RMSE between 1.2 and 2.3 ℃. The MF AC impedance method and genetic algorithm identified results reduced this error to below 1 ℃. Especially, in the genetic algorithm case, all RMSE results are lower than 0.82 ℃. Unfortunately, the LF AC impedance method failed to simulate the battery thermal dynamics. Its RMSE resulted with even higher than 16 ℃, which is unacceptable.

Usually, high and medium frequency impedances are dominated by electrochemical impedance, which corresponds to the electrochemical polarization reaction. Whereas low frequency impedances are generally dominated by diffusion impedance, which corresponds to concentration polarization reaction, and appear as diagonal lines of the Weber impedance. As time increases, concentration polarization increases.

The DC resistance is the equivalent internal resistance calculated using the instantaneous voltage drop. In the normal charging-discharging process, there is little difference with the real part of impedance in the electrochemical impedance spectroscopy. However, under the abuse conditions (such as high temperature, overcharging, etc.), even with the electrochemical side reactions neglected, the measured DC resistance is considered to be inadequate to describe the battery thermal dynamics. At Stage I, there is almost no side reaction and the internal impedance of the battery does not change much. At Stage II of overcharging, side reactions occur, and the electrochemical polarization and concentration polarization impedance increase greatly. The DC impedance can no longer reflect the actual heat generation resistance inside the battery, and the calculated heat generation is less than the actual heat generation inside. At the same time, the concentration polarization impedance appears as the Weber impedance slope. The increase in the concentration polarization impedance calculated by the electrochemical impedance spectroscopy is much greater than the increase in the electrochemical impedance, resulting with higher heat generation in the LF AC impedance spectroscopy case.

6. Conclusions

To enhance the thermal safety design, overcharging experiments are conducted to reveal the heat generation dynamics of lithium-ion batteries in this paper. Furthermore, we proposed an impedance-measurement-based electro-thermal model to simulate the battery thermal characteristics. Pulse-relaxation, electrochemical impedance methods and genetic algorithm are used for the equivalent resistance estimation. After comparing the simulation results with experimental results, it is found that medium-frequency electrochemical impedance method achieves the most accurate overcharging thermal dynamics simulation performance. A possible reason is that medium frequency impedance is mainly impacted by the polarization reactions, which dominate the overcharging process. The surface temperature simulation root mean square error is reduced to under 0.9 ℃ in all situations. The simulation results are further validated by a genetic algorithm benchmark.

This study is critical to thermal safety design of lithium-ion batteries and provides a fundamental tool for thermal runaway study. The proposed method shows much reduced computation complexity, with a potential for practical application. Our future work is to further develop a prediction scheme for lithium-ion battery thermal safety management.

Acknowledgements

The authors would like to thank the Collaborative Innovation Center of Electric Vehicles in Beijing Institute of Technology for the support of this research project. This work was also supported by Beijng Municipal Science & Technology Commission (Grant No. Z181100004618004).

References

[1] Ren D, Liu X, Feng X, Lu L, Ouyang M, Li J, et al. Model-based thermal runaway prediction of lithium-ion batteries from kinetics analysis of cell components. Appl Energy 2018;228:633–44.
[2] Feng X, He X, Ouyang M, Lu L, Wu P, Kulp C, et al. Thermal runaway propagation model for designing a safer battery pack with 25 Ah LiNixCoyMnzO2 large format lithium ion battery. Appl Energy 2015;154:74–91.
[3] Ye J, Chen H, Wang Q, Huang P, Sun J, Lo S. Thermal behavior and failure mechanism of lithium ion cells during overcharge under adiabatic conditions. Appl Energy 2016;182:464–74.
[4] Zhang C, Zhao TS, Xu Q, An L, Zhao G. Effects of operating temperature on the performance of vanadium redox flow batteries. Appl Energy 2015;155:349–53.
[5] Saw LH, Ye Y, Tay AAO. Electro-thermal analysis and integration issues of lithium ion battery for electric vehicles. Appl Energy 2014;131:97–107.
[6] Liu X, Ren D, Hsu H, Feng X, Xu G, Zhuang M, et al. Thermal runaway of lithium-ion batteries without internal short circuit. Joule 2018;2(10):2047–64.
[7] Ouyang M, Ren D, Lu L, Li J, Feng X, Han X, et al. Overcharge-induced capacity fading analysis for large format lithium-ion batteries with LiyNi1/3Co1/3Mn1/3O2 + LiyMn2O4 composite cathode. J Power Sources 2015;279:626–35.
[8] Huang P, Chen H, Verma A, Wang Q, Mukherjee P, Sun J. Non-dimensional analysis of the criticality of Li-ion battery thermal runaway behavior. J Hazard Mater 2019.
[9] A representative-sandwich model for simultaneously coupled mechanical-electrical-thermal simulation of a lithium-ion cell under quasi-static indentation tests. J Power Sour 2015;298:309–21.
[10] Li Y, Zhou Z, Wu WT. Three-dimensional thermal modeling of Li-ion battery cell and 50 V Li-ion battery pack cooled by mini-channel cold plate. Appl Therm Eng 2019;147:829–40.
[11] Esho I, Shah K, Jain A. Measurements and modeling to determine the critical temperature for preventing thermal runaway in Li-ion cells. Appl Therm Eng 2018;145:287–94.
[12] Chu Z, Feng X, Lu L, Li J, Han X, Ouyang M. Non-destructive fast charging algorithm of lithium-ion batteries based on the control-oriented electrochemical model. Appl Energy 2017;204:1240–50.
[13] Sun J, Li J, Zhou T, Yang K, Wei S, Tang N, et al. Toxicity, a serious concern of thermal runaway from commercial Li-ion battery. Nano Energy 2016;27:313–9.
[14] Cabañero MA, Altmann J, Gold L, Boaretto N, Müller J, Hein S, et al. Investigation of the temperature dependence of lithium plating onset conditions in commercial Li-ion batteries. Energy 2019;171:1217–28.
[15] Yayathi S, Walker W, Doughty D, Ardebili H. Energy distributions exhibited during thermal runaway of commercial Lithium-ion batteries used for human spaceflight applications. J Power Sour 2016;329:197–206.
[16] Shah K, Chalise D, Jain A. Experimental and theoretical analysis of a method to predict thermal runaway in Li-ion cells. J Power Sour 2016;330:167–74.
[17] Waag W, Kitz S, Sauer DU. Experimental investigation of the lithium-ion battery impedance characteristic at various conditions and aging states and its influence on the application. Appl Energy 2013;102:885–97.
[18] Mohammadian SK, Zhang Y. Improving wettability and preventing Li-ion batteries from thermal runaway using micro-channels. Int J Heat Mass Transf 2018;118:911–8.
[19] Ping P, Wang Q, Chung Y, Wen J. Modelling electro-thermal response of lithium-ion batteries from normal to abuse conditions. Appl Energy 2017;205:1327–44.
[20] Wang Q, Zhao X, Ye J, Sun Q, Ping P, Sun J. Thermal response of lithium-ion battery during charging and discharging under adiabatic conditions. J Therm Anal Calorim 2016;124(1):417–28.
[21] Feng X, Fang M, He X, Ouyang M, Lu L, Wang H, et al. Thermal runaway features of large format prismatic Lithium-ion battery using extended volume accelerating rate calorimetry. J Power Sour 2014;255:294–301.
[22] Qi C, Zhu Y, Gao F, Yang K, Jiao Q. Mathematical model for thermal behavior of lithium-ion battery pack under overcharge. Int J Heat Mass Transf 2018;124:552–63.
[23] Larsson F, Mellander BE. Abuse by external heating, overcharge and short circuiting of commercial lithium-ion battery cells. J Electrochem Soc 2014;161(10):A1611–7.
[24] Zhu X, Wang Z, Wang Y, Wang H, Wang C, Tong L, et al. Overcharge investigation of large format lithium-ion pouch cells with Li (Ni0. 6Co0. 2Mn0. 2) O2 cathode for electric vehicles: thermal runaway features and safety management method. Energy 2019;169:868–80.
[25] Feng X, Lu L, Ouyang M, Li J, He X. A 3D thermal runaway propagation model for a large format lithium-ion battery module. Energy 2016;115:194–208.

[26] Hou G, Sun Q, Ai Q, Ren X, Xu X, Guo H, et al. Growth direction control of lithium dendrites in a heterogeneous lithiophilic host for ultra-safe lithium metal batteries. J Power Sour 2019;416:141–7.
[27] Coman PT, Darcy EC, Veje CT, White RE. Modelling Li-ion cell thermal runaway triggered by an internal short circuit device using an efficiency factor and arrhenius formulations. J Electrochem Soc 2017;164(4):A587–93.
[28] Abada S, Petit M, Lecocq A, Marlair G, Moynot VS, Huet F. Combined experimental and modeling approaches of the thermal runaway of fresh and aged lithium-ion batteries. J Power Sour 2018;399:264–73.
[29] Liu H, Li J, Xie X, Wang L, He X, Ouyang M, et al. Research on overcharge safety of large-size three-element lithium-ion power battery. New Mater Ind 2015;03:48–52.
[30] Ren D, Feng X, Lu L, Ouyang M, Zheng S, Li J, et al. An electrochemical-thermal coupled overcharge-to-thermal-runaway model for Lithium-ion battery. J Power Sour 2017;364:328–40.
[31] Yuan Q, Zhao F, Wang W, Zhao Y, Liang Z, Yan D. Overcharge failure investigation of lithium-ion batteries. Electrochim Acta 2015;178:682–8.
[32] Finegan DP, Scheel M, Robinson JB, Tjaden B, Michiel MD, Hinds G, Brett DJL, Shearing PR. Investigating lithium-ion battery materials during overcharge-induced thermal runaway: an operando and multi-scale X-ray CT study. Phys Chem Chem Phys Pccp 2016;18(45):30912.
[33] Liu Y, Liu Q, Li Z, Ren Y, Xie J, He H, Xu F. Failure study of commercial LiFePO4 cells in over-discharge conditions using electrochemical impedance spectroscopy. J Electrochem Soc 2014;161(4):A620–32.
[34] Wang Z, Ma J, Zhang L. Finite element thermal model and simulation for a cylindrical Li-ion battery. IEEE Access 2017;5:15372–9.
[35] Gu W, Sun Z, Wei X, Dai H. A capacity fading model of lithium-ion battery cycle life based on the kinetics of side reactions for electric vehicle applications. Electrochim Acta 2014;133(7):107–16.
[36] Feng X, Sun J, Ouyang M, Wang F, He X, Lu L, et al. Characterization of penetration induced thermal runaway propagation process within a large format lithium-ion battery module. J Power Sour 2015;275:261–73.
[37] Bergman TL, Incropera FP, DeWitt DP, et al. Fundamentals of heat and mass transfer. John Wiley & Sons; 2011.
[38] Lopez CF, Jeevarajan JA, Mukherjee PP. Experimental analysis of thermal runaway and propagation in lithium-ion battery modules. J Electrochem Soc 2015;162(9):A1905–15.
[39] Zhang C, Jiang J, Zhang W, Liu Q, Lu Y. Electrochemical impedance model and characteristic parameters analysis of lithium-ion batteries for ladder utilization. Automat Electr Power Syst 2013;01:54–8.